Fuel Processing Technology 171 (2018) 162–172

Contents lists available at ScienceDirect

Fuel Processing Technology

journal homepage: www.elsevier.com/locate/fuproc

Research article

Numerical simulation of catalytic upgrading of biomass pyrolysis vapours in a FCC riser

Panneerselvam Ranganathan[a,*], Sai Gu[b,*]

[a] Environmental Technology Division, CSIR–National Institute of Interdisciplinary Science and Technology (CSIR–NIIST), Trivandrum, India
[b] Chemical and Process Engineering, University of Surrey, United Kingdom

ARTICLE INFO

Keywords:
Biomass
Biofuels
Pyrolysis vapours
FCC riser
CFD
Upgrading

ABSTRACT

Catalytic upgrading of biomass pyrolysis vapours is a potential method for the production of hydrocarbon fuel intermediates. This work attempts to study the catalytic upgrading of pyrolysis vapours in a pilot scale FCC riser in terms of hydrodynamics, residence time distribution (RTD) and chemical reactions by CFD simulation. NREL's Davison Circulating Riser (DCR) reactor was used for this investigation. CFD simulation was performed using 2-D Eulerian–Eulerian method which is computationally less demanding than the alternative Euler-Lagrangian method. First, the hydrodynamic model of the riser reactor was validated with the experimental results. A single study of time-averaged solid volume fraction and pressure drop data was used for the validation. The validated hydrodynamic model was extended to simulate hydrodynamic behaviours and catalyst RTD in the Davison Circulating Riser (DCR) reactor. Furthermore, the effects on catalyst RTD were investigated for optimising catalyst performance by varying gas and catalyst flow rates. Finally, the catalytic upgrading of pyrolysis vapours in the DCR riser was attempted for the first time by coupling CFD model with kinetics. A kinetic model for pyrolysis vapours upgrading using a lumping kinetic approach was implemented to quantify the yields of products. Five lumping components, including aromatic hydrocarbons, coke, non–condensable gas, aqueous fraction, and non–volatile heavy compounds (residue) were considered. It was found that the yield of lumping components obtained from the present kinetic model is very low. Thus, the further research needs to be carried out in the area of the kinetic model development to improve the yield prediction.

1. Introduction

Fast pyrolysis, the rapid heating of biomass in the oxygen–free atmosphere, has been considered as a promising technology for the production of transportation fuels, speciality and fine chemicals, and furnace and boiler fuel [1]. Unfortunately, the produced bio-oil from fast pyrolysis of biomass has a highly complex mixture of oxygenated compounds that considered unsuitable for direct use in existing liquid hydrocarbon fuel technologies such as fractionation units (atmospheric and vacuum distillation), fluid catalytic cracking (FCC), thermal cracking, and hydroprocessing units. The issue thus related to raw pyrolysis bio–oil can be upgraded or treated by catalytic method [2]. Catalytic fast pyrolysis (CFP) has a potential option for improving the quality of organic products from fast pyrolysis of biomass [3]. This process can be operated by either in–situ where the catalyst and biomass are mixed in the same reactor or ex–situ where the vapours from the biomass pyrolysis reactor react with the catalyst in a separate reactor system [4,5]. Ex–situ catalytic fast pyrolysis process or pyrolysis vapours upgrading can be considered a potential method for the production of hydrocarbon fuel intermediates such as carboxylic acids, aldehydes, ketones, furans and phenolic compounds [6]. The chemical reactions occurring in ex–situ catalytic fast pyrolysis include deoxygenation, hydrogen transfer, aromatisation, isomerisation, and C—C coupling reactions [7]. Deoxygenation reaction can be achieved via decarboxylation – removal of oxygen as CO_2, decarbonylation – removal of oxygen as CO, and hydrodeoxygenation – removal of oxygen as H_2O. Hydrogen transfer reaction can occur at atmospheric pressure and at high reaction temperatures without hydrogen [7]. C—C coupling reactions can be achieved via transalkylation (methyl transfer), ketonisation, aldol condensation, and hydroalkylation reactions. Mostly, the ex–situ CFP has been conducted in either micro–scale via Pyro–GC–MS [8–10] or in lab–scale reactor [11–13]. The lab–scale reactor of pyrolysis vapours upgrading was performed in either a fixed bed or fluidised bed reactors. In comparison with fixed bed reactor, fluidised bed operations could be preferred because it produces relatively lesser coke and thus reduces catalyst deactivation [14]. Also, it has the advantages of continuous and quick catalyst regeneration [6]. The pyrolysis vapours upgrading in fluidised bed follows a similar procedure in the

* Corresponding authors.
E-mail addresses: pranganathan@niist.res.in (P. Ranganathan), sai.gu@surrey.ac.uk (S. Gu).

https://doi.org/10.1016/j.fuproc.2017.11.008
Received 10 April 2017; Received in revised form 30 October 2017; Accepted 16 November 2017
Available online 23 November 2017

petroleum industry with the reactor concept of fluid catalytic cracking (FCC). In a typical FCC unit, catalyst from the regenerator enters at the bottom of the riser where it reacts with the feed in the riser and is separated from the gaseous products by the cyclone. The catalyst flows back to the regenerator where the air is injected to burn off the coke that is deposited on the active surface of the catalyst.

In literature, various fundamental studies have already been conducted to understand the underlying mechanism of pyrolysis vapours upgrading and coking process using different microporous catalysts and several process parameters such as feedstock type (pine, red oak, and hybrid poplar) and temperature (400–700 °C) [8–10]. Among the various catalysts tested, HZSM–5 based catalyst is widely applied for the catalytic upgrading of pyrolysis vapours due to its strong acidity, shape selectivity, and ion exchange capacity. However, HZSM–5 deactivates rapidly due to the decrease in its acid sites (Si/Al ratio) [9]. To study catalyst activity during vapours upgrading, Mukarakate et al. [8] have investigated in a horizontal quartz annular flow reactor coupled with a molecular beam mass spectrometer. They have found the deactivation of the catalyst completely at a biomass–to–catalyst ratio of about 3. Wan et al. [9] have investigated the effect of Si/Al ratio and the temperature on the catalytic activity using a CDS analytical pyroprobe with a small packed-bed flow reactor. The reactor has the dimension of 6″ long and ¼″ OD. They have found the higher aromatic yield for HZSM–5 with Si/Al ratio of 40 at 500 °C. Another study has also reported the pyrolysis vapours upgrading in a micro-pyrolyser by investigating the effect of feedstock properties (type: hybrid poplar; size: 0.2–3 mm; and loading: 0.5 mg), and catalyst temperature (400–700 °C) and loading (10–40 mg) [10]. To investigate how the catalyst type influences the vapours upgrading, a lab-scale reactor was also used in the literature. Park et al. [11] have studied the upgrading of pine pyrolysis vapours in a lab–scale fixed catalytic bed reactor using different zeolite catalysts such as HZSM–5, H–Y, and Ga–ZSM–5. They have also investigated the influence of bed temperature, vapours residence time, and catalyst composition on the product distribution. Iliopoulou et al. [15] have reported the catalytic upgrading of pyrolysis vapours in the pilot–scale riser using two different catalysts of FCC catalyst and ZSM–5 based FCC additive catalyst. Though the investigation of pyrolysis vapours cracking has been studied mainly at the lab-scale in the literature, it possesses many challenges at the industrial-scale that need to be addressed. As discussed by Yildiz et al. [16], the challenges include operation mode, life and deactivation of catalyst, and novel process configurations.

The issues related to the cracking of pyrolysis vapours over the catalyst are the lower yield of bio–oil, the higher yield of gas, and high coking rate resulting in rapid deactivation of the catalyst. The formation of coke is mainly from the polymerisation of aromatic hydrocarbon or condensation of unreacted pyrolysis vapours. This is due to low effective H/C ratio of the pyrolysis vapours [8]. The higher yield of gas is due to a heavy fraction of oxygenated compounds in pyrolysis vapours removed as CO_2, CO, and H_2O(g) through decarboxylation, decarbonisation, and hydrodeoxygenation reactions, respectively. Therefore, to retain carbon in the pyrolysis vapours, the reaction pathways involved in the removal of oxygen heteroatom from the pyrolysis vapours need to be optimised [7,14]. Also, the contact time between the catalyst and vapours in the riser need to be optimised [15]. Typical vapours residence time in the fluidised bed riser is to be 2–3 s. However, the longer contact time between catalyst and vapours may form the excessive coking and thus reduce the catalyst activity [8]. The catalyst deactivation due to the deposition of coke on the active surface of catalyst depends on the type of catalyst, reactor configuration, and process conditions. In the view of reactor configuration, it is important to understand the underlying fluid dynamics of the reactor to improve the catalyst performance. Thus, the present study motivates to develop a computational model for the pyrolysis vapours upgrading in the fluidised bed riser. Different modelling approaches have been developed in the literature for studying the hydrodynamics of FCC riser along with reaction kinetic modelling. These approaches are: (i) 1–D hydrodynamic model with lumped kinetics; (ii) 1–D hydrodynamic model with molecular–level kinetics; (iii) 2–D empirical hydrodynamics with the lumping kinetics; (iv) CFD model with the lumping kinetics; and (v) CFD model with molecular–level kinetics [17]. Among them, first three methods are computationally easy to solve with less accuracy, whereas highly detailed information of flow fields and reaction kinetics can be obtained from CFD model with molecular–level kinetics. However, it requires a lot of computational efforts. Most widely used method is CFD with the lumping kinetic modelling, which is more comprehensive and requires a reasonable computational cost with adequate accuracy. In addition, this method has been applied to the crude oil cracking in the FCC riser [18,19] and fast pyrolysis of biomass for biofuel production [20–22].

The present work aims to simulate the hydrodynamics of pyrolysis vapours and catalyst in a Davison Circulating Riser. The Davison Circulating Riser (DCR) is the industry standard FCC pilot–scale reactor developed by Grace's [23]. The National Renewable Energy Laboratory (NREL) has recently studied biomass pyrolysis vapours upgrading using the Davison Circulating Riser (DCR) [12,24]. In which, the vapours were fed to continuously circulating catalyst for hydrocarbon production without adding hydrogen. It has advantages of continuous coke removal to keep the catalyst in the active form. In this work, the hydrodynamic characteristics of pyrolysis vapours and HZSM-5 catalyst in the riser are calculated using 2-D Eulerian–Eulerian approach. Using hydrodynamic results, the prediction of catalyst residence time in the riser is performed for studying the contact time of vapours with the catalyst. This is examined by the effect of catalyst feed rate and gas flow rate on the hydrodynamic behaviour and catalyst residence time distribution (RTD). Furthermore, the hydrodynamic model is extended to simulate the catalytic upgrading of pyrolysis vapours by a coupled CFD–lumping (pseudo–components model) kinetic approach. Five lumps of the major products in pyrolysis upgrading, including aromatic hydrocarbons, coke, non–condensable gas, aqueous fraction, and non–volatile heavy compounds (residue) are considered.

The rest of the paper is organised as follows. Section 2 describes the modelling approaches with governing equations used for predicting the flow fields in the riser and Section 3 describes the numerical methodology and solution algorithm implemented in this study. The results obtained from this study are discussed in Section 4. The conclusions drawn from this numerical study are presented in the final section of the paper.

2. CFD modelling

Ensemble averaged conservation equations of mass, momentum, and energy were used to describe the flow fields of catalyst and pyrolysis vapours in the riser. All phases are described as interpenetrating continua in an Eulerian frame of reference. Gas phase is treated as a continuous phase which consists of pyrolysis vapours and nitrogen. It is worth to mention that aerosol is also formed during the pyrolysis process and is carried through together with vapours. However, it is not included in the gas phase mixture to avoid the complexity of the model. A catalyst particle is considered as the dispersed solid phase.

2.1. Hydrodynamic equations

The continuity equation for gas (g) and particle phases (p) can be written as [25]

$$\frac{\partial}{\partial t}(\alpha_g \rho_g) + \nabla \cdot (\alpha_g \rho_g \vec{v_g}) = S_g \tag{1}$$

$$\frac{\partial}{\partial t}(\alpha_p \rho_p) + \nabla \cdot (\alpha_p \rho_p \vec{v_p}) = S_p \tag{2}$$

where ρ, α, and $\vec{v}$ are the density, the volume fraction and the

phase–averaged velocity and S is the source term due to chemical reactions.

The momentum equation for gas and particle phases can be written as

$$\frac{\partial}{\partial t}(\alpha_g\rho_g\vec{v_g}) + \nabla\bullet(\alpha_g\rho_g\vec{v_g}\vec{v_g}) = -\alpha_g\nabla P + \alpha_g\rho_g\vec{g} + \nabla\bullet\bar{\bar{\tau}}_g + \beta(\vec{v_p} - \vec{v_g}) \tag{3}$$

$$\frac{\partial}{\partial t}(\alpha_p\rho_p\vec{v_p}) + \nabla\bullet(\alpha_p\rho_p\vec{v_p}\vec{v_p}) = -\alpha_p\nabla P - \nabla p_p + \alpha_p\rho_p\vec{g} + \nabla\bullet\bar{\bar{\tau}}_p - \beta(\vec{v_p} - \vec{v_g}) \tag{4}$$

where g is the acceleration due to gravity, P is the pressure shared by all phases, p_p is the solid pressure, and β is the interfacial momentum exchange coefficient between the solid and the gas phases.

The gas phase stress tensor, $\bar{\bar{\tau}}_g$ can be written as

$$\bar{\bar{\tau}}_g = \alpha_g\mu_g(\nabla\vec{v_g} + \nabla\vec{v_g}^T) + \alpha_g\left(\lambda_g - \frac{2}{3}\mu_g\right)\nabla\bullet\vec{v_g}\bar{\bar{I}} \tag{5}$$

where $\mu_g = \mu_{gl} + \mu_{gt}$, μ_g is the gas phase shear viscosity, μ_{gl} is the gas phase laminar viscosity, λ_g is the gas phase bulk viscosity, and μ_{gt} is the gas phase turbulence viscosity, calculated based on the k–ε turbulence model and is given by

$$\mu_{gt} = 0.09\rho_g\frac{k^2}{\varepsilon} \tag{6}$$

The value of k and ε was obtained directly from the transport equations of the turbulence kinetic energy and turbulence dissipation rate.

The particle stress tensor, $\bar{\bar{\tau}}_p$ in Eq. (4) can be written as

$$\bar{\bar{\tau}}_p = \alpha_p\mu_p(\nabla\vec{v_p} + \nabla\vec{v_p}^T) + \alpha_p\left(\lambda_p - \frac{2}{3}\mu_p\right)\nabla\bullet\vec{v_p}\bar{\bar{I}} \tag{7}$$

where μ_p is the solid shear viscosity, and λ_p is the solid bulk viscosity.

The drag force between the gas and solid phases was modelled as

$$\beta = \frac{3}{4}C_D\frac{\alpha_p\alpha_g\rho_g\,|\vec{v_p} - \vec{v_g}|}{d_p}\alpha_g^{-2.65}H_d \text{ when } \alpha_g \geq 0.4 \tag{8}$$

$$\beta = 150\frac{\alpha_p(1-\alpha_g)\mu_g}{\alpha_g d_p^2} + 1.75\frac{\rho_g\alpha_p\,|\vec{v_p} - \vec{v_g}|}{d_p} \text{ when } \alpha_g < 0.4 \tag{9}$$

where C_D is the drag coefficient exerted by the dispersed solid phase on the gas phase and is obtained by

$$C_D = \frac{24}{\alpha_g Re_p}[1 + 0.15(\alpha_g Re_p)^{0.687}] \tag{10}$$

where d_p is the particle diameter, C_D is the drag coefficient of a single particle in a stagnant fluid and Re_p is the particle Reynolds number and is defined as

$$Re_p = \frac{\rho_g d_p(\vec{v_p} - \vec{v_g})}{\mu_g} \tag{11}$$

The heterogeneous index in Eq. (8), H_d is given in Table 1 [26].

The solids pressure due to solid–solid collisions was modelled using the kinetic theory granular flow. The model equation is given as [27]

$$p_p = \alpha_p\rho_p\Theta_p + 2\rho_p(1 + e_{pp})\,\alpha_p{}^2 g_{0,pp}\Theta_p \tag{12}$$

where e_{pp} denotes the coefficient of restitution for solid–solid collisions, $g_{0,\,pp}$ denotes the radial distribution function, and Θ_p denotes the granular temperature.

The equation of the radial distribution function is given as

$$g_{0,pp} = \left(1 - \left(\frac{\alpha_p}{\alpha_{p,\max}}\right)^{1/3}\right)^{-1} \tag{13}$$

In Eq. (13), the maximum solid packing, $\alpha_{p,\,\max}$ was 0.63.

Solid shear viscosity, μ_p is expressed as

$$\mu_p = \mu_{p,col} + \mu_{p,kin} + \mu_{p,fr} \tag{14}$$

$$\mu_{p,col} = \frac{4}{5}\alpha_p\rho_p d_p g_{0,pp}(1 + e_{pp})\left(\frac{\Theta_p}{\pi}\right)^{1/2}\alpha_p \tag{15}$$

$$\mu_{p,kin} = \frac{10\rho_p d_p\sqrt{\pi\Theta_p}}{96\alpha_p(1 + e_{pp})g_{0,pp}}\left[1 + \frac{4}{5}(1 + e_{pp})g_{0,pp}\alpha_p\right]^2\alpha_p \tag{16}$$

$$\mu_{p,fr} = \frac{p_s\sin\phi}{2\sqrt{I_{2D}}} \tag{17}$$

where ϕ is the angle of internal friction, and $\sqrt{I_{2D}}$ is the second invariant of the deviatoric stress tensor.

Solid bulk viscosity, λ_p is given as [28]

$$\lambda_p = \frac{4}{3}\alpha_p\rho_p d_p g_{0,pp}(1 + e_{pp})\left(\frac{\Theta_p}{\pi}\right)^{1/2} \tag{18}$$

In this work, the granular temperature was determined from solving transport equations derived from kinetic theory and is given as [28]

$$\frac{3}{2}\left[\frac{\partial}{\partial t}(\alpha_p\rho_p\Theta_p) + \nabla\bullet(\alpha_p\rho_p\vec{v_p}\Theta_p)\right] = (-P_p\bar{\bar{I}} + \bar{\bar{\tau}}_p)\colon\nabla\vec{v_p} + \nabla\bullet(k_{\Theta_p}\nabla\Theta_p) - \gamma_{\Theta_p} + \phi_{gp} \tag{19}$$

where γ_{Θ_p}, k_{Θ_p}, and ϕ_{gp} represent the collision dissipation of energy, the diffusion coefficient, and the energy exchange between the gas and particle phase, respectively and are given by [28]

$$\gamma_{\Theta_p} = \frac{12(1 - e_{pp}^2)g_{0,pp}}{d_p\sqrt{\pi}}\rho_p\alpha_p{}^2\Theta_p{}^{3/2} \tag{20}$$

$$\phi_{gp} = 3\beta\overline{\Theta} \tag{21}$$

$$k_{\Theta_p} = \frac{150\rho_p d_p\sqrt{\pi\Theta_p}(1 - e_{pp}^2)}{384(1 + e_{pp})g_{0,pp}}\left[1 + \frac{6}{5}(1 + e_{pp})g_{0,pp}\alpha_p\right]^2 + 2\rho_p d_p\alpha_p{}^2 g_{0,pp}(1 + e_{pp})\sqrt{\frac{\Theta_p}{\pi}} \tag{22}$$

The energy equations for each phase, considering negligible of pressure work, kinetics terms and viscous heating, can be written as

$$\frac{\partial}{\partial t}(\alpha_g\rho_g h_g) + \nabla\bullet(\alpha_p\rho_p\vec{v_p}h_p) = \alpha_p\frac{\partial p_p}{\partial t} + \bar{\bar{\tau}}_g\colon\nabla\vec{v_g} - \nabla\bullet\vec{q_g} + \Delta H_g + h_{pg}(T_p - T_g) \tag{23}$$

$$\frac{\partial}{\partial t}(\alpha_p\rho_p h_p) + \nabla\bullet(\alpha_p\rho_p\vec{u_p}h_p) = \alpha_p\frac{\partial p_p}{\partial t} + \bar{\bar{\tau}}_p\colon\nabla\vec{v_p} - \nabla\bullet\vec{q_p} + \Delta H_p - h_{pg}(T_p - T_g) \tag{24}$$

where h is the specific enthalpy, $\vec{q}$ is the heat flux, ΔH is the heat of reaction, h_{pg} is the volumetric heat exchange coefficient between the solid and the gas phases.

The heat transfer coefficient between the phases provided by Gunn [29] is given by

$$h_{pg} = \frac{6k_g\alpha_g\alpha_p Nu_p}{d_p^2} \tag{25}$$

and

$$Nu_p = (7 - 10\alpha_g + 5\alpha_g^2)(1 + 0.7Re_p^{0.2}Pr^{1/3}) + (1.33 - 2.4\alpha_g + 1.2\alpha_g^2)Re_p^{0.7}Pr^{1/3} \tag{26}$$

Table 1
The formulae for heterogeneous index (H_d) in EMMS drag model [26].

Fitting formula ($H_d = a(Re_p + b)^c$, $0.001 \le Re_p \le 35$)	Range ($\varepsilon_{mf} \le \varepsilon_g \le 1$)
$a = 0.8526 - \frac{0.5846}{1 + (\varepsilon_g/0.4325)^{22.6279}}$ $b = 0.0$ $c = 0.0$	$0.4 \le \varepsilon_g \le 0.46$
$a = 0.032 + \frac{0.7399}{1 + (\varepsilon_g/0.4912)^{54.4265}}$ $b = 0.00225 + \frac{777.0074}{1 + 10^{(\varepsilon_g - 0.3987)66.3224}} + \frac{0.02404}{1 + 10^{(0.5257 - \varepsilon_g)53.8948}}$ $c = 0.1705 - \frac{0.1731}{1 + (\varepsilon_g/0.5020)^{37.7091}}$	$0.46 < \varepsilon_g \le 0.545$
$a = (2124.956 - 2142.3\varepsilon_g)^{-0.4896}$ $b = (0.8223 - 0.1293\varepsilon_g)^{13.0310}$ $c = \frac{(\varepsilon_g - 1.0013)}{-0.06633 + 9.139(\varepsilon_g - 1.0013) + 6.9231(\varepsilon_g - 1.0013)^2}$	$0.545 < \varepsilon_g \le 0.99$
$a = 0.4243 + \frac{0.8800}{1 + \exp\left(\frac{-(\varepsilon_g - 0.9942)}{0.00218}\right)}\left(1 - \frac{1}{1 + \exp\left(\frac{-(\varepsilon_g - 0.9989)}{0.00003}\right)}\right)$ $b = 0.01661 + 0.2436\exp\left(-0.5\left(\frac{\varepsilon_g - 0.9985}{0.00191}\right)^2\right)$ $c = 0.0825 - 0.0574\exp\left(-0.5\left(\frac{\varepsilon_g - 0.9979}{0.00703}\right)^2\right)$	$0.99 < \varepsilon_g \le 0.9997$

2.2. Residence time distribution (RTD) modelling

Residence time distribution (RTD) represents the degree of mixing of phases which directly relates the hydrodynamics of the riser. This can thus be an important parameter to evaluate the reactor performance in terms of conversion and selectivity of chemical reactions. It is generally characterised as a probability density function, $E(t)$ curve which relates the concentration, $C(i)$ in each sample, i along the sampling period and is given by

$$E(i) = \frac{C_i}{\sum_{i=0}^{\infty} C_i \Delta t_i} \tag{27}$$

The mean residence time and variance of statistical moments of $E(t)$ can be calculated as

$$\bar{t} = \int_0^{\infty} tE(t)dt \approx \sum_{i=0}^{\infty} t_i E(t_i)\Delta t_i \tag{28}$$

$$\sigma_t^2 = \sum_{i=0}^{\infty} (t_i - \bar{t})^2 E(t_i)\Delta t_i \tag{29}$$

Thus, the dimensionless form of the variance to measure the degree of dispersion can be calculated as

$$\sigma_\theta = \frac{\sigma_t}{\bar{t}} \tag{30}$$

In this work, Eulerian based species transport equation was chosen for studying catalyst RTD. This method calculates RTD based on the convective velocity of the catalyst, $\vec{v_p}$, which can be calculated reasonably [30]. In this approach, few tracer particles are injected per unit time into main flow fields in the riser which is similar to the impulse–stimulus response technique used in the practical work. The concentration of injected tracer is monitored at the outlet of the riser that can provide RTD curve.

A transport equation for a tracer particle in the solid phase can be written as

$$\frac{\partial}{\partial t}(\alpha_p \rho_p Y^p_{tracer}) + \nabla\cdot(\alpha_p \rho_p \vec{v_p} Y^p_{tracer}) = \nabla\cdot(\alpha_p \rho_p D^p_{tracer} \nabla Y^p_{tracer}) \tag{31}$$

where $Y_{tracer}{}^P$ is the mass fraction of tracer in the solid phase and $D_{tracer}{}^P$ is the diffusion coefficient for tracer in the mixture, which was considered as $2.88e-05$ m^2/s. A similar range of value of 2.8291e-05 m^2/s was estimated from the measured RTD data by Hua et al. [30].

2.3. Kinetic modelling

A lumping kinetic model was used to study the catalytic upgrading of pyrolysis vapours over HZSM–5 catalyst. This method is useful for simplifying the complex reaction mechanism involved in pyrolysis vapours cracking. A comprehensive lumping kinetic model for bio–oil cracking with HZSM-5 constructed based on the reaction pathways proposed by Adjaye and Bakhshi [31] is shown in Fig. 1. It is shown in the scheme that some of the heavy fraction in the bio–oil, mainly macromolecular oxygenated compounds, are cracked into the lower oxygenates and olefins through deoxygenation and cracking reactions. On the other hand, some of these heavy organics deposit on the catalyst surface and undergo polymerisation to form coke and residue. The residue is non–volatile heavy fraction in bio-oil, which does not evaporate during vacuum distillation. The cracked products of various carbon fragments undergo oligomerisation to produce a mixture of C_2—C_{10} olefins. These olefins then subsequently are converted to hydrocarbons through a series of reaction of aromatisation, alkylation, and isomerisation. During these reactions, some of the aromatic hydrocarbons also undergo polymerisation to form coke and residue. The kinetic modelling is useful for determining the appropriate operating conditions that can be used to predict the yield of upgraded bio–oil products. Adjaye and Bakhshi [32] have developed a rate based kinetic modelling of bio–oil upgrading using the proposed reaction pathways (Fig. 1). They have used the power-law form of the rate equation to obtain the reaction rate constant, the activation energy, and the reaction order, considering six major products of organic distillate fraction, aqueous fraction, gas, coke, residue, and hydrocarbons. In the present work, five lumps, such as the aqueous fraction, coke, gas, organic liquid (volatiles), and residue (non–volatiles), were only considered since hydrocarbon is the component of organic fraction. The kinetic parameters for each lumping component are shown in Table 2.

It can be seen from the table that the lower activation energy (3 kJ/

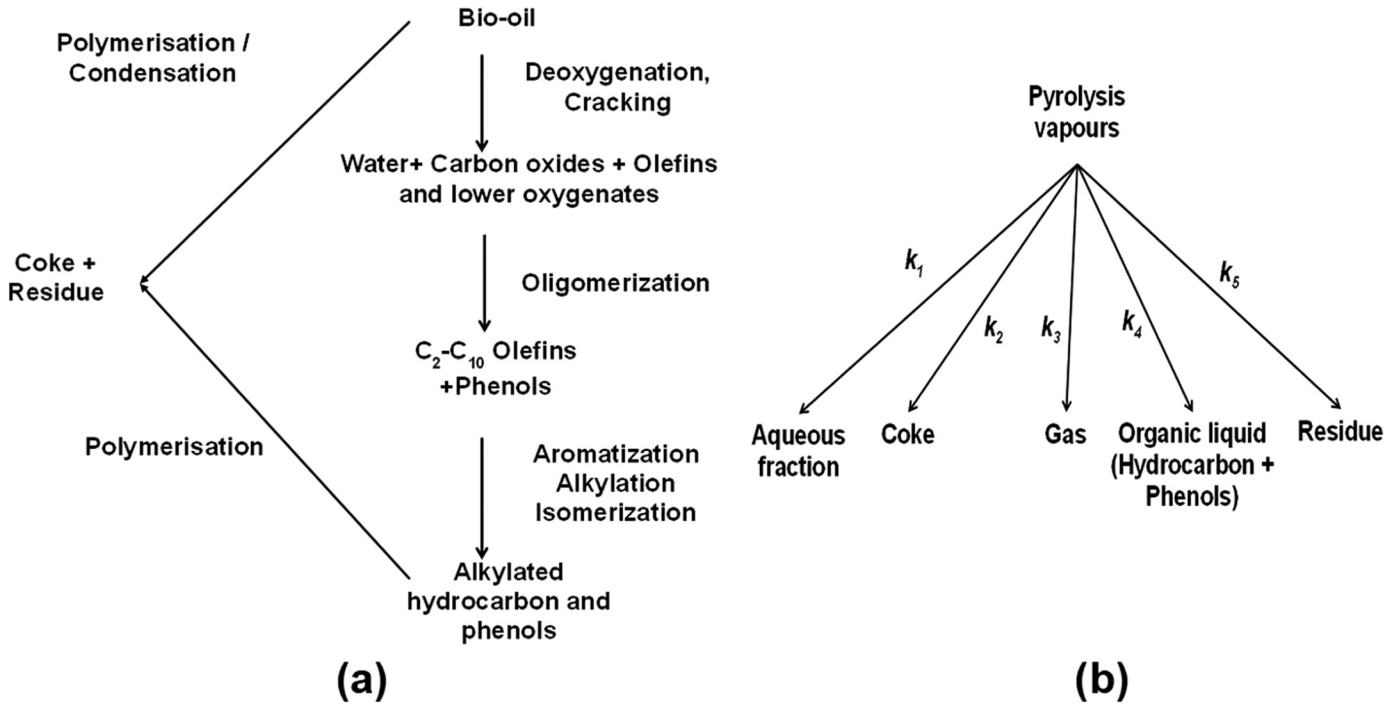

Fig. 1. Schematic representation of (a) proposed reaction pathways (b) lumping compounds for conversion of bio-oil through HZSM-5 catalyst [31].

Table 2
Kinetic parameters of bio-oil upgrading at 410 °C [32].

Rate of a reaction (k)	Activation energy, E (kJ/mol)	Reaction order	Pre-exponential facor, k_o
k_1	79	1.4	0.6e − 05
k_2	61	1.2	7.5e − 05
k_3	38	0.8	18e − 05
k_4	3	0.9	80e − 05
k_5	61	0.7	37e − 05

mol) is observed for the organic fraction, whereas the formation of aqueous fraction requires the highest activation energy (79 kJ/mol).

To model the cracking of pyrolysis vapours, a species transport equation was used. This can be written as

$$\frac{\partial}{\partial t}(\alpha_g \rho_g Y_i^g) + \nabla\cdot(\alpha_g \rho_g \vec{v_g} Y_i^g - (\alpha_g \rho_{gp} D_i^g \nabla Y_i^g)) = S_i \quad (32)$$

where Y_i^g is the mass fraction of species, i in the gas phase and S_i is the net production of species, i due to chemical reaction.

3. Numerical methodology

A fluid dynamic behaviour of pyrolysis vapours and catalyst in the riser was simulated using ANSYS Fluent v14.0. To validate the hydrodynamic model of the fluidised bed riser, the experimental results from Particulate Solid Research, Inc. (PSRI) experimental research facility in Chicago [33] were considered. The dimension of PSRI reactor was the diameter of 0.2 m and height of 14.2 m. More details of the experimental setup are found in Table 3. A sketch of simulated 2–D DCR reactor with the boundary details is shown in Fig. 2. The reason for choosing NREL's DCR in this study is only lab/pilot-scale riser reactor data available in the literature for pyrolysis vapours upgrading. The DCR riser has a diameter of 0.01 m and the height of 3 m. A 2–D unsteady-state simulation was performed to reduce the computational cost. Inlet boundary condition was employed at the bottom of the bed to specify a uniform inlet of a gas mixture of diluted pyrolysis vapours and nitrogen. The solid inlet was specified on the side of the riser at the bottom. The pressure value was specified in the outlet boundary condition at the top of the reactor. The lateral walls were modelled using the no–slip velocity boundary conditions for the gas phase and the free–slip boundary conditions for the solid phase. More details of the boundary conditions are depicted in Table 4. The coupled partial differential form of transport equations was converted to discrete algebraic governing equations by finite volume method. The advection scheme of second–order upwind for momentum equation and QUICK scheme for the volume fraction equation were used. Time derivatives in the governing equations were integrated with second–order implicit scheme with a time step of 0.0001 s. Total time for each simulation was 50 s and the time-averaged quantities were calculated from the simulation time of 20–50 s as the simulation results stabilised approximately at 20 s. Pressure–velocity coupling was achieved by the phase–coupled SIMPLE algorithm. The residual based convergence criteria used in all the simulations was 1×10^{-4}. The maximum number of iterations used for each time step was around 50.

Table 3
Experimental parameters used in the present study.

Properties	PSRI [33]	Davison Circulating Riser (DCR) [24]
Diameter of riser, m	0.2	0.01
Height of riser, m	14.2	3
Particle diameter	76 μm	75 μm
Particle density	1712 kg/m^3	1500 kg/m^3
Gas viscosity	1.8e-05 kg/m^3	1.8e − 05 kg/m^3
Gas density	1.2 kg/m^3	1.2 kg/m^3
Gas inlet velocity	5.2 m/s	1.0; 1.45 m/s
Solid mass flux	489 kg/(m^2 s)	1.68, 2.4, 4.5, 13.2, 27 kg/(m^2 s)
Solid inlet velocity	0.714 m/s	0.0028, 0.004; 0.0075; 0.022; 0.045 m/s
initial static bed height, m	0.2	–
Solid inlet volume fraction	0.4	0.4

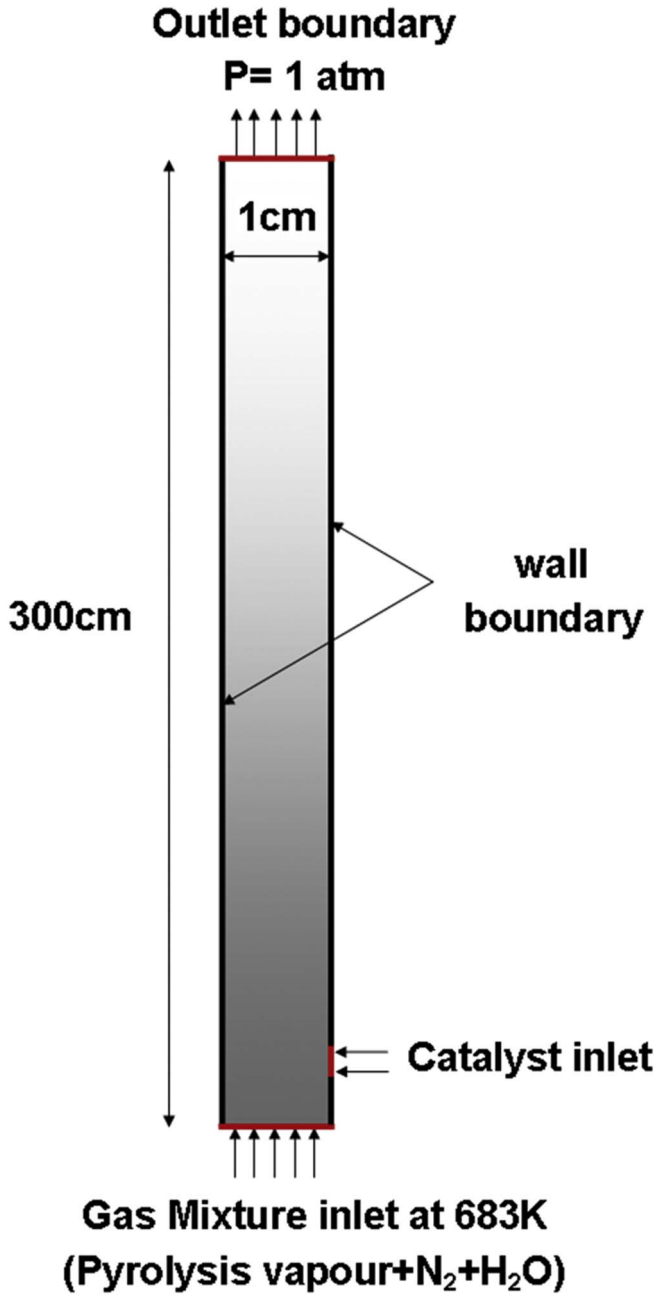

Fig. 2. Schematic representation of DCR geometry with boundary conditions [20].

Table 4
Boundary details for hydrodynamics modelling of DCR.

Boundary	Phase	Species	Mass fraction (wt%)
Bottom inlet	Gas phase	Pyrolysis vapours	0.5
		Nitrogen	0.5
	Solid phase	HZSM-5 catalyst	0
Side inlet	Gas phase	Pyrolysis vapours	0
		Nitrogen	0.6 (volume fraction)
	Solid phase	HZSM-5 catalyst	0.4 (volume fraction)
Outlet	Pressure outlet (0 Pa)		

4. Results and discussion

The validation of hydrodynamic results of the riser reactor is discussed first. Then, the validated numerical simulations are extended to investigate the hydrodynamics of the pyrolysis vapours and catalyst flows, residence time distribution (RTD), and catalytic cracking of pyrolysis vapours in the DCR reactor.

4.1. Hydrodynamic validation

In this section, CFD simulation was performed without considering chemical reactions in the riser. The hydrodynamic behaviour of gas–solid flows in the riser was validated using the experimental data of PSRI reactor [33]. Solid particle of Geldart A type with the size of 76 μm and a density of 1712 kg/m^3 was used. The hydrodynamics of gas–solid flows were studied for predicting time-averaged radial volume fraction at various axial positions of the riser using γ–ray densitometer. First, a mesh dependency study was carried out to choose the optimum mesh size in the simulation. Three meshes of 20 × 1420, 40 × 1420 and 50 × 1890 were used. Simulation results of time-averaged solid volume fraction along the radial position at the height of 8.1 m and the pressure drop along the riser for the solid mass flux of 489 kg/m^2 s were compared with the experimental result of the PSRI reactor [33], which are shown in Fig. 3a, b, respectively. It can be seen from Fig. 3a that both medium and coarse meshes show a more or less similar trend which matches with the experimental data mostly in the core region of the riser. The fine grid results match with the experimental data in the annular region of the riser whereas it overpredicts in the core region of the riser. Overall, all of three meshes show a similar trend. In the view of computational accuracy and efficiency, the medium grid was used in the further simulation. The axial profiles of pressure drop per unit length predicted by three meshes are shown in Fig. 3b. The results from both coarse and medium grids relatively match with the experimental data at the top region of the riser. However, the profile observed in both coarse and medium meshes deviates from the S-shaped curve of the experimental data. The fine grid shows the S-shaped curve, which slightly deviates from the experimented data. The discrepancies in both radial and axial profiles predicted by CFD model are also reported in the literature [34,35]. These discrepancies can be attributed to the selection of closure models, such as drag and gas-phase turbulence, which need further improvement for coarse-grid riser simulations.

4.2. Hydrodynamic behaviour of NREL's DCR reactor

In this section, the local hydrodynamics of solid bed expansion behaviour in NREL's DCR reactor are discussed. The fluidisation gas contains a mixture of pyrolysis vapours and nitrogen. HZSM–5 based zeolite catalyst with a particle size of 75 μm and the density of 1500 kg/m^3 was used in this study which is the Geldart A type. The solid enters the riser at the right side of the riser only with the opening of 0.01 m wide. Two sides solid inlet configuration shown the better prediction of the hydrodynamic behaviours reported in the literature is not tested in this study [36]. The inlet composition of a gas mixture is shown in Table 4. Initially, a mesh dependency study was performed. Three mesh sizes of 0.0005 × 0.002, 0.0005 × 0.0015 and 0.0005 × 0.001 with the total elements of 20 × 1500, 20 × 2000 and 20 × 3000, respectively were used. Results of mean solid volume fraction and mean axial solid velocity along the radial position at the axial position of 1.5 m in the DCR reactor obtained from three meshes are shown in Fig. 4. These simulations were carried out at a gas velocity of 1.0 m/s with the solid velocity of 0.045 m/s. It can be seen that all of three meshes give a comparatively similar trend for both mean solid volume fraction and mean axial solid velocity and can thus be referred approximately as grid-independent solutions. To trade-off between the computing time and accuracy, a medium mesh size of 0.0005 × 0.0015 was used for further simulation. Fig. 5 shows solid bed expansion behaviour in the riser at a gas velocity of 1.0 m/s with the solid velocity of 0.045 m/s, which is having the biomass pyrolysis vapours to catalyst ratio of 20 (reactive components in the inlet pyrolysis vapours only considered). The simulation was performed for the total of time of 50 s. It can be

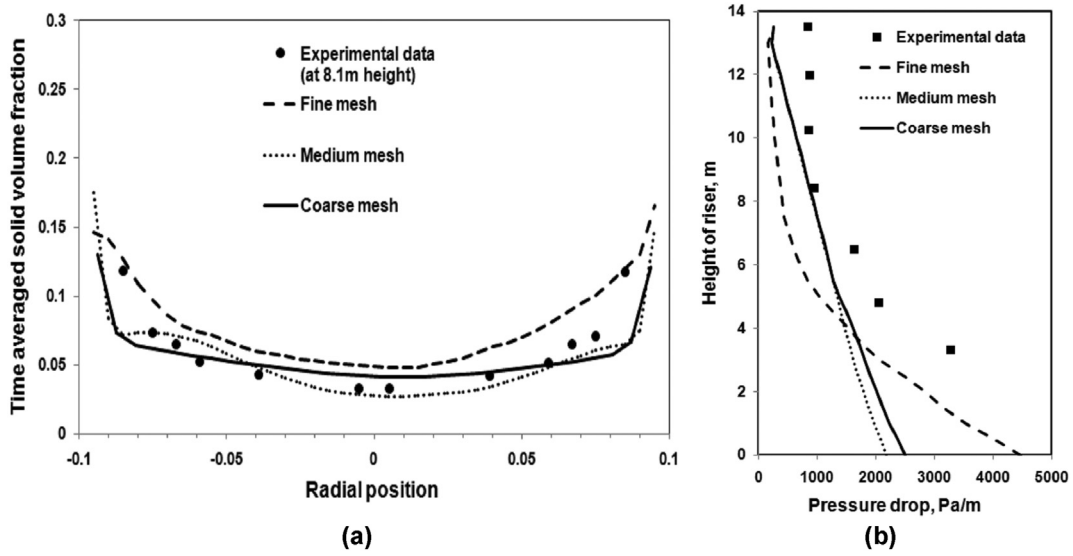

Fig. 3. Mesh dependency study on (a) radial profile of time averaged solid volume fraction (b) axial profile of pressure drop in the PSRI riser.

seen from the figure that the bed particles begin to expand in the riser with some particles hitting the wall and falling when gas was introduced into the bottom of the riser. It is also found from the figure that the large clusters of the solid particle are observed along the length of the riser which tends to congregate near the wall where the momentum of the carrier gas is very low. The cluster of particles was formed by the agglomeration of small particles which affect fluidisation characteristics and residence time distribution (RTD). Also, it can be noted from the figure that the particles are starting to leave the bed around at $t = 10$ s.

As shown in Fig. 6 in the lower section of the riser (1.5 m), the particles exhibit a larger volume fraction near the wall and smaller volume fraction in the centre. The particle volume fraction at the wall is approximately 1.5 times than that in the riser centre. The particle concentration profile follows the gas velocity profile, i.e., in the riser centre, the high gas velocity exhibits a greater transport and entrainment capacity, resulting in a diluted particle distribution. At the higher section of the riser (at 2.5 m), the solid volume fraction profiles show a slightly lower than that in the lower section of the riser. The non-uniform distribution of particle concentration would influence the cracking reactions in the FCC riser.

Time-averaged axial particle velocity along with the dimensionless radial position in the riser is shown in Fig. 7 at the height of 2 m for two different solid velocities at a particular gas velocity of 1.0 m/s. This plot shows the different trend for different solid velocity. For a high solid inlet velocity, the time-averaged axial velocity of particles at the centre of the reactor shows higher in comparison with a low inlet solid

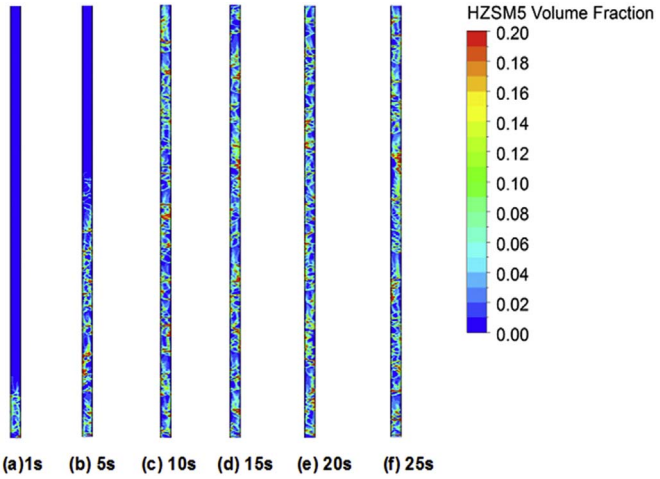

Fig. 5. Solid bed expansion behaviour in the DCR riser at a gas velocity of 1.0 m/s with the solid velocity of 0.045 m/s.

velocity. The raised particles due to the upward flowing gas in the centre try to come down along the side of the reactor and thus negative velocity is observed near to the wall of the reactor.

4.3. Catalyst RTD in NREL's DCR reactor

In gas–solid riser, solid mixing behaviour can be significantly

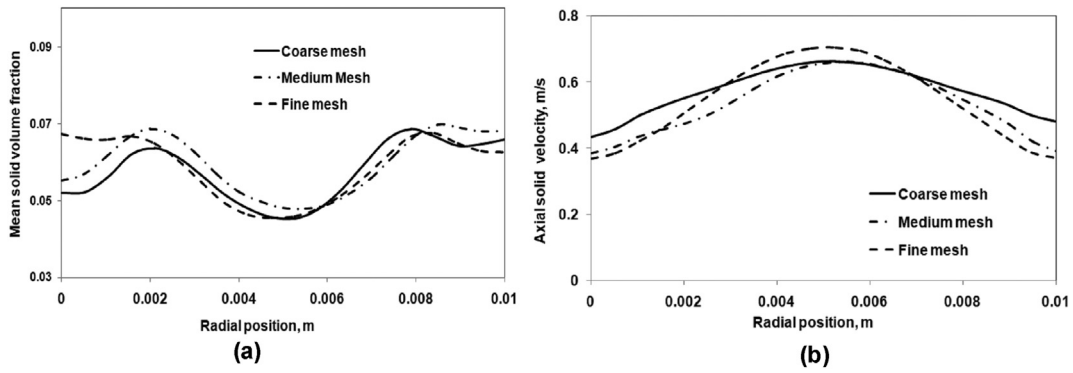

Fig. 4. Mesh dependency study on (a) radial profile of mean solid volume fraction (b) radial profile of mean axial solid velocity in the DCR riser.

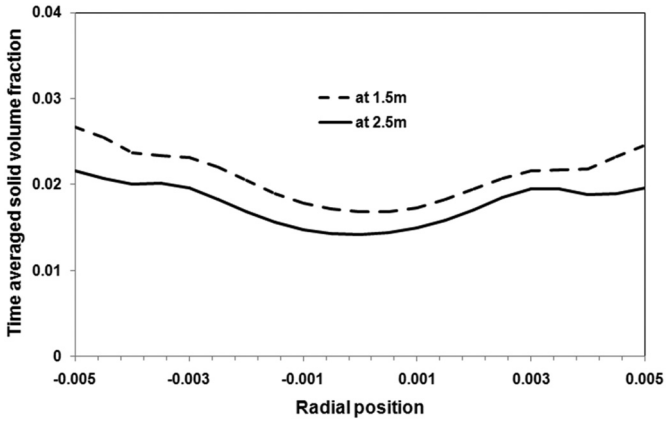

Fig. 6. Time-averaged solid volume fraction profile at various heights of the riser at a gas velocity of 1.0 m/s with the solid velocity of 0.0075 m/s.

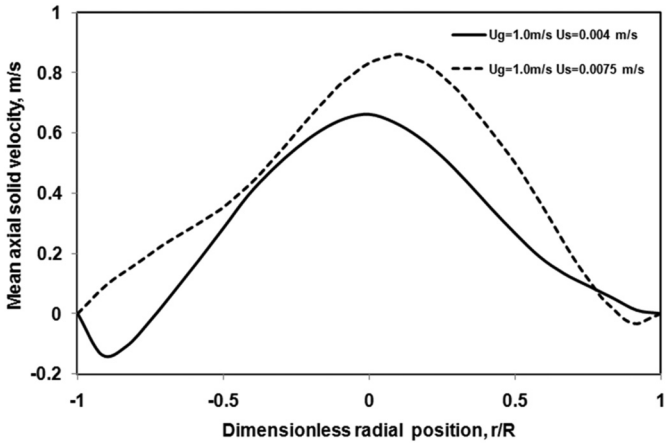

Fig. 7. Radial profiles of time-averaged mean axial solid velocity for different solid inlet velocities.

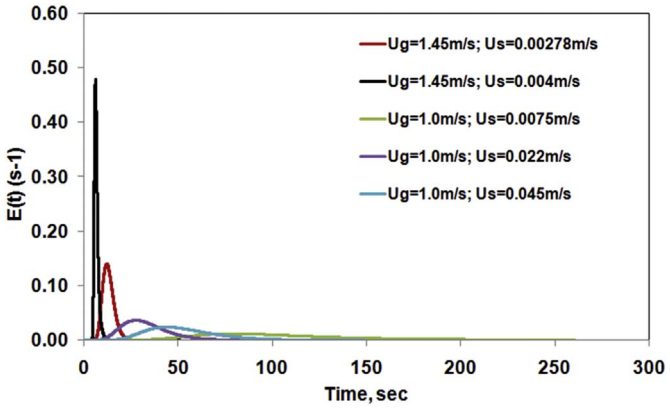

Fig. 8. Effect of the solid velocity on solid RTD in DCR riser for different gas and particle velocities.

influenced the conversion and selectivity of the reaction. Therefore, it is important to understand the solid mixing behaviour in the riser. Solid mixing is usually studied to predict RTD by injecting tracer particles into the riser reactor. In this study, tracer particles were injected into the riser reactor at the solid inlet for the period of 1 s. In a recent study of Hua et al. [30], various injection times starting from 0.1–3 s were studied and concluded that the injection time did not influence the solid RTD significantly. Thus, the present study was employed the injection time of 1 s with the sampling time interval of 0.01 s. The tracer properties were set similar to catalyst properties. Flow fields from the

Table 5
Catalyst residence time distribution for different operating conditions.

Conditions		RTD, $\bar{t}$ s	Dimensionless variance, σ_θ
Gas velocity, m/s	Solid velocity, m/s		
1.45	0.00278	11.5	0.21
1.45	0.004	7.5	0.49
1.00	0.0075	105	0.413
1.00	0.022	32.8	0.37
1.00	0.045	52.76	0.362

hydrodynamic simulation were used as an input for RTD calculation. The concentration of tracer at the outlet was monitored. Fig. 8 presents catalyst RTD curve ($E(t)$ curve) obtained for the different gas and solid velocities. It can be seen from the figure that for the gas velocity of 1.45 m/s with two different solid velocities of 0.00278 and 0.004 m/s the shape of the RTD in the riser follows the close to a plug flow behaviour, i.e., almost all the particles in the riser have a uniform distribution due to all the particles moving the same velocity. However, for the case of the gas velocity of 1.0 m/s with different solid velocities the shapes of the curve show a long tail. This may be due to the occurrence of solids back–mixing in the riser. Generally, solids back–-mixing is more significant in both annular and bottom regions of the riser due to the formation of particle clusters in these regions. From $E(t)$ curve data, the mean residence time, $\bar{t}$ and dimensionless variance, σ_θ were calculated using Eqs. (28) and (30) respectively, for various conditions, which are shown in Table 5. It is found that with the high solid and gas velocities mean residence time of catalyst is shorter. In pyrolysis vapours upgrading, too short of a contact time between vapours and solids may lead to the lower conversion and too long leads to the excessive coking and the deactivation of the catalyst or undesirable products. Thus, the optimised contact time between vapours and catalyst is necessary for improving the process. The dimensionless variance, σ_θ in Table 5 shows that the flow state in the reactor shows towards to the plug-flow condition when the solid velocity increases, i.e., when σ_θ approaches to 1, the flow in the reactor can be expected to be close to a plug-flow state. This behaviour is also discussed in the literature [30]. Fig. 9 shows the contours of tracer mass fraction in the riser at various times in the case of the gas velocity of 1.45 m/s and solid velocity of 0.00278 m/s. This figure clearly shows the process of the motion of tracer particle in the riser, including the propagation and the escape, as the time goes on.

4.4. Catalytic upgrading in NREL's DCR reactor

In this section, a catalytic upgrading of pyrolysis vapours with

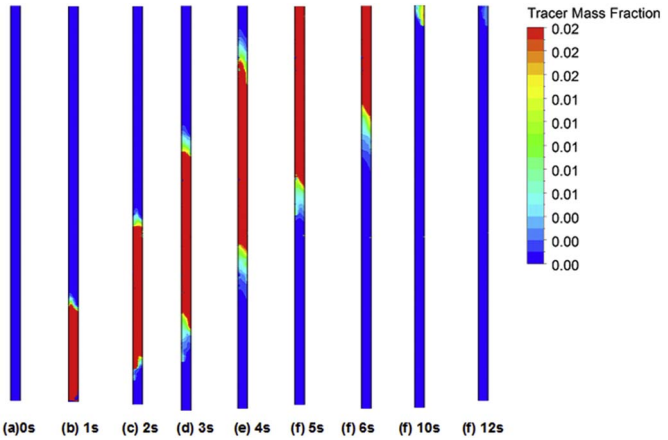

Fig. 9. Contours of tracer mass fraction in the DCR riser at a gas velocity of 1.45 m/s with the solid velocity of 0.00278 m/s.

Table 6
Averaged quantities of lumped compounds at temperature of 410 °C for various cases.

Lumped compounds	Model compounds	Inlet mass fraction of pyrolysis vapours	Outlet mass fraction			
			u_g = 1.45 m/s u_s = 0.00278 m/s	u_g = 1.45 m/s u_s = 0.004 m/s	u_g = 1.00 m/s u_s = 0.022 m/s	u_g = 1.00 m/s u_s = 0.045 m/s
Pyrolysis vapours (volatile)	Gas with molecular weight of 78 kg/kg mol	0.3115	0.310	0.310	0.303	0.303
Aqueous fraction	H_2O	0	1.484e − 13	1.485e − 13	1.88e − 13	2.04e − 13
Coke	Carbon	0	3.14e − 10	1.39e − 10	7.29e − 12	1.54e − 11
Gas	CO_2	0	3.44e − 07	3.45e07	4.55e − 07	4.84e − 07
Hydrocarbon	Benzene	0	0.00076	0.00077	0.001	0.0011
Residue (heavy non-volatile)	Limonene	0.1885	0.1884	0.1883	0.1842	0.186

HZSM–5 based zeolite is discussed. A pseudo component based a lumping kinetic modelling along with CFD was implemented in this study. Five pseudo–species were incorporated into hydrodynamic modelling. The model components of corresponding lumping components and their inlet composition are shown in Table 6. It is assumed that the inlet pyrolysis vapours contain only volatile and non-volatile (residue). In this simulation, the diluted pyrolysis vapours mass fraction and the inert gas of nitrogen mass fraction were fixed at 0.5. This simulation was carried out at the reaction temperature of 410 °C which is the maximum temperature for which the kinetic parameters are reported by Adjaye and Bakhshi [32]. The physical property of pyrolysis vapours, such as the density calculated based on the volume-averaged mixing law, the viscosity of 1.72e − 05 kg/(m s), and molecular weight of 78 g/mol, was defined in this study. The total time used in this simulation was 50 s. A mass fraction of various lumping components during upgrading of pyrolysis vapours obtained from CFD simulation for different gas and solid velocities (both lower and higher solid mean residence time) is shown in Table 6. It can be seen from the table that the mass fraction of all lumping components at the outlet of the riser reactor for different conditions shows a more or less similar value. This indicates that the cracking kinetics of pyrolysis vapours in the riser reactor predicted by the present model show insignificant.

The contours of lumping components mass fraction and their mass fraction profiles along the height of the riser are shown in Figs. 10 and 11 respectively. It can be seen from Fig. 11 that the mass fraction of gas, water vapours, coke, and aromatics in the riser increases with increasing the height of the riser. About 0.2% of aromatic hydrocarbon yield and the negligible amount of coke, aqueous, and gas yields are observed at the outlet of the riser. The mass fraction of pyrolysis vapours and residue in the riser decreases quickly up to the height of 0.25 m and reaches a stabilised value. The mass fraction of pyrolysis vapours decreases from 0.31 to 0.303 in the riser, indicating that the conversion of pyrolysis vapours during upgrading is very low, about 2.25%. This may be due to the kinetics of vapours cracking used in this study not correctly to quantify the yield of various components. Also, in developing the kinetic model, Adjaye and Bakhshi [32] have used the condensed phase of bio–oil in their experiments, which was later vapourised and flowed into catalytic bed for upgrading. This implies that the proposed kinetic model of bio-oil cracking is not suitable for pyrolysis vapours cracking. Furthermore, the temperature in the riser influences the product distribution [14]. In this study, the temperature (410 °C) in the riser was very low. In most of the upgrading of pyrolysis vapours reported in the literature, the reaction was carried out at above 500 °C [12,14].

Thus, it is worth saying that the present kinetic model may not suitable for the upgrading of vapours directly from biomass pyrolysis.

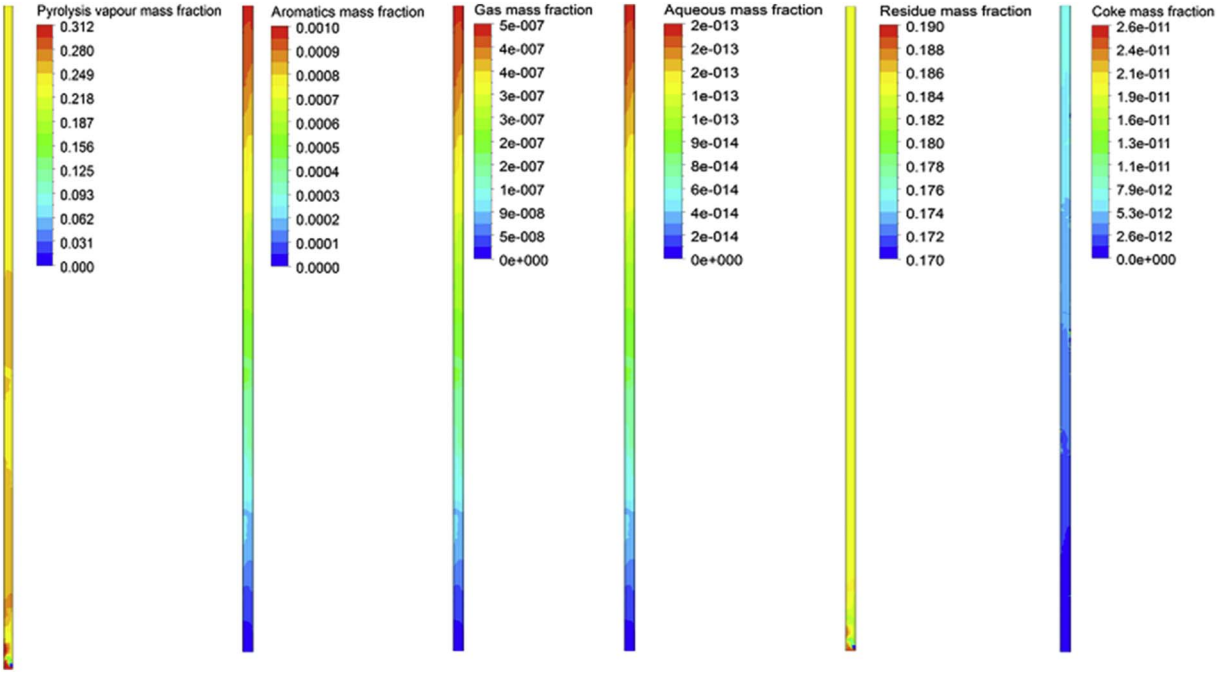

Fig. 10. Contour of lumping species mass fraction during catalytic upgrading of vapours in the DCR riser for a gas velocity of 1.0 m/s and solid velocity of 0.045 m/s at the reactor temperature of 410 °C.

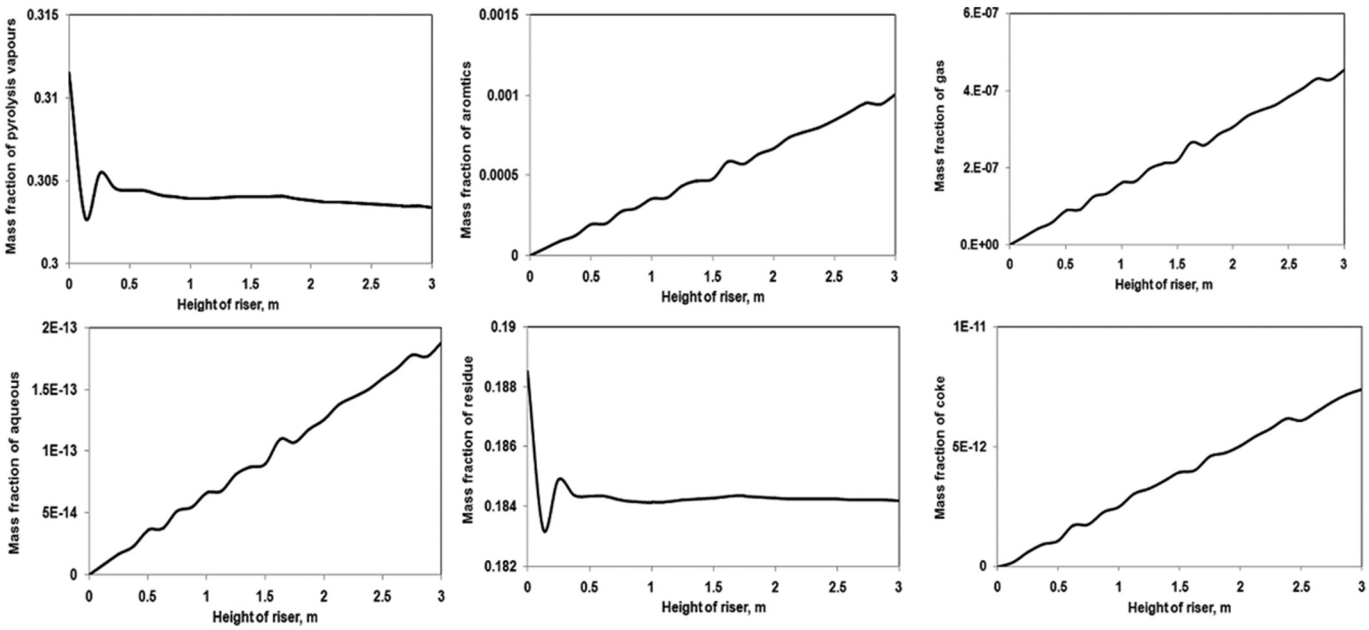

Fig. 11. Axial profile of the various lumping species mass fractions for a gas velocity of 1.00 m/s and solid velocity of 0.045 m/s at the reactor temperature of 410 °C.

Therefore, a kinetic model needs to be developed for predicting the lumping components yield in pyrolysis vapours upgrading. This may need a development of a global kinetic model or detailed first-principles based microkinetic model for a coupled reaction–transport simulation in the pyrolysis vapours cracking. It is also important to mention that the assigned model compound for each lumping component may influence the kinetic modelling of pyrolysis vapours upgrading. Thus, the issue related to the assigning model compound for each lumping component needs also to be verified.

5. Conclusions

In this work, the hydrodynamic behaviour of pyrolysis vapours and catalyst flows in a pilot–scale FCC riser by CFD simulation was studied. NREL's Davison Circulating Riser (DCR) reactor was used for this investigation. Hydrodynamic modelling results of the riser were validated with PSRI experimental data. Using the validated CFD model, the hydrodynamics and the catalyst RTD in the DCR were performed. Furthermore, the effects on catalyst RTD were investigated for various operating conditions to optimise the catalyst performance. For catalytic cracking of pyrolysis vapours, multiphase flow CFD model with five lumping pseudo–components based kinetic model was attempted for the first time. It was found that the yield of lumping components obtained from the present kinetic model is very low. Thus, further research will be required for the development of the kinetic model to improve the yield of lumping components. This involves a development of a global kinetic model or detailed first-principles based microkinetic model for coupled reaction–transport simulation in pyrolysis vapours upgrading. Overall, this preliminary study can be helpful to understand the fluid dynamics of pyrolysis vapours and catalyst flows to improve the performance of catalytic upgrading in the FCC riser. Also, this study can be provided the guidance related to the operating conditions that needed for pyrolysis vapours upgrading.

Nomenclature

C_D	drag coefficient between solid and gas phase, dimensionless
d_p	particle mean diameter, m
$D_{i,m}$	diffusion coefficient for species, i in mixtures, m^2/s
$D_{tracer,m}$	diffusion coefficient for tracer particle in mixtures, m^2/s
E	RTD curve parameter, s^{-1}
e_{pp}	coefficient of restitution for solid–solid collisions, dimensionless
$g_{0,\ pp}$	radial distribution function, dimensionless
h_{pg}	heat transfer coefficient, J/(s m K)
h	specific enthalpy, J/kg
H_d	heterogeneous index, dimensionless
k_0	pre–exponential factor for reaction constant
k	liquid phase turbulence kinetic energy, m^2/s^2
k_g	gas phase thermal conductivity, W/m K
Nu_p	Nusselt number, dimensionless
P	liquid–phase pressure, kg/(m s^2)
p_p	pressure of solid phase, kg/(m s^2)
Pr	Prandtal number, dimensionless
$\vec{q}$	heat flux, J/s m^2
Re_p	particle Reynolds number, dimensionless
t	time, s
$\tilde{t}$	mean residence time, s
T	temperature of reactor, K
T_g	gas temperature, K
T_p	particle temperature, K
$\vec{v}_g$	local gas velocity vector, m/s
$\vec{v}_p$	local particle velocity vector, m/s
Y_i^g	mass fraction of species i in the gas phase, dimensionless
$Y_{tracer}{}^p$	mass fraction of tracer in the particle phase, dimensionless

Greek letters

α_g	gas volume fraction, dimensionless
α_p	volume fraction of particle phase p, dimensionless
$\alpha_{p,\ max}$	maximum solid packing, dimensionless
ε	liquid phase turbulence eddy dissipation, m^2/s^3
ρ_g	gas density, kg/m^3
ρ_p	density of particle phase p, kg/m^3
μ_g	gas phase viscosity, kg/m s^2
μ_{gl}	gas phase laminar viscosity, kg/(m s)
μ_{gt}	gas phase turbulence viscosity, kg/(m s)
μ_p	solid shear viscosity, kg/(m s)
λ_p	solid bulk viscosity, kg/(m s)
β	interfacial momentum exchange coefficient, kg/(m^3 s)
$\bar{\bar{\tau}}_g$	fluid stress tensor, kg/(m s^2)
$\bar{\bar{\tau}}_p$	particle stress tensor, kg/(m s^2)

Θ_p	granular temperature, m^2/s^2
γ_{Θ_p}	collision dissipation of energy, kg/(m s^3)
k_{Θ_p}	diffusion coefficient, m^2/s
ΔH	heat of reaction
ϕ	angle of internal friction
ϕ_{gp}	energy exchange between the gas and particle phase

Subscripts and superscripts

g	gas phase
p	particle phase

Acknowledgement

Authors gratefully acknowledge the financial support for this work by the UK Engineering and Physical Sciences Research Council (EPSRC) projects (EP/K036548/2; EP/J020184/2). Author (PR) thanks to DST, India for the financial support by DST INSPIRE Faculty Award (DST/INSPIRE/2014/ENG-97).

References

[1] A.V. Bridgwater, Review of fast pyrolysis of biomass and product upgrading, Biomass Bioenergy 38 (2012) 68–94.
[2] J. Diebold, J. Scahill, Biomass to Gasoline (BTG): upgrading pyrolysis vapours to aromatic gasoline with zeolite catalysis at atmospheric pressure, ACS Symp. Ser. (1988) 264–276.
[3] R.H. Venderbosch, A critical view on catalytic pyrolysis of biomass, ChemSusChem 8 (2015) 1306–1316.
[4] M. Biddy, A. Dutta, S. Jones, A. Meyer, Ex–situ catalytic fast pyrolysis technology pathway, National Renewable Energy Lab Report, 2013, p. 717.
[5] M. Biddy, A. Dutta, S. Jones, A. Meyer, In-situ catalytic fast pyrolysis technology pathway, National Renewable Energy Lab Report, 2013, p. 716.
[6] S. Wan, Y. Wang, A review on ex situ catalytic fast pyrolysis of biomass, Front. Chem. Sci. Eng. 8 (2014) 280–294.
[7] C. Liu, H. Wang, A.M. Karim, J. Sun, Y. Wang, Catalytic fast pyrolysis of lignocellulosic biomass, Chem. Soc. Rev. 43 (2014) 7594–7623.
[8] C. Mukarakate, X. Zhang, A.R. Stanton, D.J. Robichaud, P.N. Ciesielski, K. Malhotra, B.S. Donohoe, E. Gjersing, R.J. Evans, D.S. Heroux, R. Richards, K. Iisa, M.R. Nimlos, Real-time monitoring of the deactivation of HZSM-5 during upgrading of pine pyrolysis vapours, Green Chem. 16 (2014) 1444–1461.
[9] S. Wan, C. Waters, A. Stevens, A. Gumidyala, R. Jentoft, L. Lobban, D. Resasco, R. Mallinson, S. Crossley, Decoupling HZSM-5 catalyst activity from deactivation during upgrading of pyrolysis oil vapors, ChemSusChem 8 (2015) 552–559.
[10] K. Wang, P.A. Johnston, R.C. Brown, Comparison of in-situ and ex-situ catalytic pyrolysis in a micro-reactor system, Bioresour. Technol. 173 (2014) 124–131.
[11] H.J. Park, H.S. Heo, J.K. Jeon, J. Kim, R. Ryoo, K.E. Jeong, Y.K. Park, Highly valuable chemicals production from catalytic upgrading of radiata pine sawdust-derived pyrolytic vapours over mesoporous MFI zeolites, Appl. Catal. B Environ. 95 (2010) 365–373.
[12] G. Yildiz, M. Pronk, M. Djokic, K.M. van Geem, F. Ronsse, R. van Duren, W. Prins, Validation of a new set-up for continuous catalytic fast pyrolysis of biomass coupled with vapour phase upgrading, J. Anal. Appl. Pyrolysis 103 (2013) 343–351.
[13] B.A. Black, W.E. Michener, K.J. Ramirez, M.J. Biddy, B.C. Knott, M.W. Jarvis, J. Olstad, O.D. Mante, D.C. Dayton, G.T. Beckham, Aqueous stream characterization from biomass fast pyrolysis and catalytic fast pyrolysis, ACS Sustain. Chem. Eng. 4 (2016) 6815–6827.
[14] O.D. Mante, F.A. Agblevor, Catalytic conversion of biomass to bio-syncrude oil, Biomass Convers. Biorefin. 1 (2011) 203–215.
[15] E.F. Iliopoulou, S. Stefanidis, K. Kalogiannis, A.C. Psarras, A. Delimitis, K.S. Triantafyllidis, A.A. Lappas, Pilot-scale validation of Co-ZSM-5 catalyst performance in the catalytic upgrading of biomass pyrolysis vapours, Green Chem. 16 (2014) 662–674.
[16] G. Yildiz, F. Ronsse, R. van Duren, W. Prins, Challenges in the design and operation of processes for catalytic fast pyrolysis of woody biomass, Renew. Sust. Energ. Rev. 57 (2016) 1596–1610.
[17] Y. Peng Du, Q. Yang, H. Zhao, C. He Yang, An integrated methodology for the modeling of Fluid Catalytic Cracking (FCC) riser reactor, Appl. Petrochem. Res. 4 (2014) 423–433.
[18] J. Gao, C. Xu, S. Lin, G. Yang, Y. Guo, Advanced model for turbulent gas–solid flow and reaction in FCC riser reactors, AICHE J. 45 (1999) 1095–1113.
[19] Y. Behjat, S. Shahhosseini, M.A. Marvast, CFD analysis of hydrodynamic, heat transfer and reaction of three phase riser reactor, Chem. Eng. Res. Des. 89 (2011) 978–989.
[20] K. Papadikis, S. Gu, A.V. Bridgwater, CFD modelling of the fast pyrolysis of biomass in fluidised bed reactors. Part B: heat, momentum and mass transport in bubbling fluidised beds, Chem. Eng. Sci. 64 (2009) 1036–1045.
[21] A. Sharma, S. Wang, V. Pareek, H. Yang, D. Zhang, Multi-fluid reactive modeling of fluidized bed pyrolysis process, Chem. Eng. Sci. 123 (2015) 311–321.
[22] P. Ranganathan, S. Gu, Computational fluid dynamics modelling of biomass fast pyrolysis in fluidised bed reactors, focusing different kinetic schemes, Bioresour. Technol. 213 (2016) 333–341.
[23] K. Bryden, G. Weatherbee, E. Thomas Habib, Flexible pilot plant technology for evaluation of unconventional feedstocks and processes, Grace Catalysts Technologies Catalagram (2013) 1–19.
[24] J. Zieler, M. Nimlos, R. Grout, D. Robichaud, T. Foust, S. Pannala, Using 3D simulation to calculate FCC catalyst residence time distribution in a pilot-scale circulating riser reactor for pyrolysis vapour upgrading, TCBiomass 2014, Denver CO, 2014.
[25] Ansys–Fluent Inc., Fluent Users Manual Version 14.0, (2012) (New Hampshire, USA).
[26] B. Lu, W. Wang, J. Li, Searching for a mesh-independent sub-grid model for CFD simulation of gas–solid riser flows, Chem. Eng. Sci. 64 (2009) 3437–3447.
[27] C.K.K. Lun, S.B. Savage, D.J. Jeffrey, N. Chepurniy, Kinetic theories for granular flow: inelastic particles in couette flow and slightly inelastic particles in a general flow field, J. Fluid Mech. 140 (1984) 223–256.
[28] D. Gidaspow, Multiphase Flow and Fluidisation: Continuum and Kinetic Theory Descriptions, Academic Press, Boston, 1994.
[29] D.J. Gunn, Transfer of heat or mass to particles in fixed and fluidized beds, Int. J. Heat Mass Transf. 21 (1978) 467–476.
[30] L. Hua, J. Wang, J. Li, CFD simulation of solids residence time distribution in a CFB riser, Chem. Eng. Sci. 117 (2014) 264–282.
[31] J.D. Adjaye, N.N. Bakhshi, Production of hydrocarbon by catalytic upgrading of a fast pyrolysis bio-oil. Part II: comparative catalyst performance and reaction pathways, Fuel Process. Technol. 45 (1995) 185–202.
[32] J.D. Adjaye, N.N. Bakhshi, Catalytic conversion of a biomass-derived oil to fuels and chemicals II: chemical kinetics, parameter estimation and model predictions, Biomass Bioenergy 8 (1995) 265–277.
[33] T. Knowlton, D. Geldart, J. Matsen, D. Kind, Comparison of CFB hydrodynamic models, PSRI Challenge Problem at the Eight International Fluidisation Conference, France, 1995.
[34] S. Benyahia, On the effect of subgrid drag closures, Ind. Eng. Chem. Res. 49 (2010) 5122–5131.
[35] M.T. Shah, R.P. Utikar, V.K. Pareek, M.O. Tade, G.M. Evans, Effect of closure models on Eulerian–Eulerian gas–solid flow predictions in riser, Powder Technol. 269 (2015) 247–258.
[36] M.T. Shah, R.P. Utikar, G.M. Evans, M.O. Tade, V.K. Pareek, Effect of inlet boundary conditions on computational fluid dynamics (CFD) simulations of gas-solid flows in risers, Ind. Eng. Chem. Res. 51 (2012) 1721–1728.